IOSR Journal of Applied Chemistry (IOSR-JAC)
e-ISSN: 2278-5736.Volume 17, Issue 5 Ser. 1 (May 2024), PP 27-42
www.iosrjournals.org

Synthesis And Characterization Of Biochar–Carbon Nanotubes Composite And Its Adsorptive Capacity For Rhodamine B Dye

Mutembei K. Mutuma, Eric M. Njogu And Joel M. Gichumbi
Department Of Chemistry, Multimedia University Of Kenya, P. O. Box 15653 Nairobi – 00503, Kenya
Department Of Physical Sciences, Chuka University, P. O Box 109 – 60400 Chuka.

Abstract
Water scarcity and pollution are major challenges in the world today. The major water pollutants include heavy metals, pesticides, dioxins, furans, phenolics, and dyes. Consumption of these pollutants triggers the emergence of diseases, including cancer in both humans and animals. Dyes are colored pollutants that hinder photosynthesis and increase the biochemical oxygen demand (BOD) by preventing the penetration of light in water. They get into the water bodies through the disposal of untreated and partially treated wastewater by agricultural and industrial processes. Therefore, there is a need for an affordable and effective technique for water treatment. Adsorption is proven to be the superior technique compared to the others, as it is easy to design, reusability, and effectiveness in removing a wide range of pollutants from aqueous solutions. The adsorbents used should be abundant, affordable, and with the desired adsorption properties. In addition, they should be porous, with high specific surface area and high binding capabilities. Water hyacinths used in this study possess these properties; it is abundant, have low economic value, and are porous. On the other hand, nanotechnology offers a high surface area and high adsorption capacities, among others. This study investigates the efficiency of water hyacinth's biochar–multiwalled carbon nanotubes (MWCNTs) nanocomposite to adsorb Rhodamine B from water. The adsorbent's functional groups, structural, and morphological properties were characterized using Fourier Transform Infrared Spectroscopy (FTIR), X-ray Diffraction (XRD), and Transmission Electron Microscopy (TEM). The adsorption percentages for hyacinth's biochar (stem and leaves), 2.5:97.5% MWCNT–biochar, and 5:95% MWCNT–biochar for Rhodamine B were determined to be 36%, 66%, and 75%, respectively. Adsorption was optimal after 2 hours of contact time, for 400 ppm of the adsorbate, 1.6g of the adsorbent, solution pH 3, and at room temperature (~ 25 °C). The data fitted better on the pseudo-second-order and Freundlich models.
Keywords: *Adsorption, Rhodamine B, Biochar-MWCNT Nanocomposite*

Date of Submission: 16-04-2024 Date of Acceptance: 26-05-2024

I. Introduction

Water scarcity is a major global challenge today. The available water is significantly polluted due to the increasingly growing population and industries. The increase in industries, particularly in developing countries has influenced the emission of toxic gases and channeling untreated or partially treated wastewater into the environment [1-8]. This is due to the lack of affordable and effective water treatment techniques [9, 10].

The major water pollutants include heavy metals (lead, cadmium, copper, zinc, and nickel), pesticides (lindane, Aldrin, and dieldrin), dioxins, furans, phenolics, and dyes [1, 8, 11]. When released into the water bodies, they greatly affect the aquatic ecosystem, vegetation, and water quality. Colored pollutants such as dyes also prevent the penetration of light, which hinders photosynthesis and increases the biochemical oxygen demand (BOD) [1, 2, 4, 5, 8, 12]. The majority of dyes persist in the environment due to their properties, including high solubility, high migration, and high thermal stability [7, 13].

Broadly, dyes are categorized into basic, acidic, disperse, direct, reactive, sulphur, and metal complex dyes [14]. Basic dyes such as rhodamine B (RhB) are among the readily available and widely used class of dyes. However, they carry a high risk to human and animal health [15, 16]. For example, RhB is carcinogenic [15]. Despite this, it is still used in the textile, soap, food, and paper industries, among others [15]. Currently, the techniques available for removing RhB from wastewater have low efficiencies [14]. This begs for a superior and affordable technique for maximum removal of RhB from the wastewater. This study investigates the efficiency of cross-linked hyacinth's (stem and leaves) biochar–multiwalled carbon nanotubes (MWCNTs) composite in removing RhB from water. Biochar is a material rich in carbon that is prepared by the decomposition of biomass in an enclosed chamber with little or no oxygen.

RhB is a cationic dye with a chemical formula $C_{28}H_{31}ClN_2O_3$ and a molecular weight of 479.01 grams/mole [17]. The structural formula for RhB is indicated in Figure 1 [15].

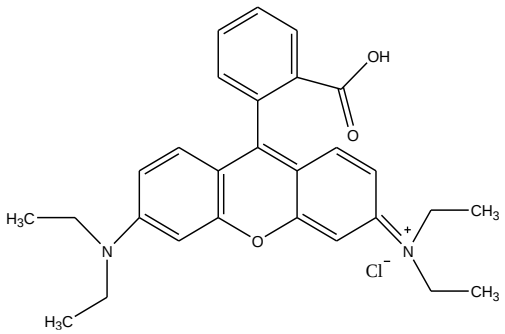

Figure 1: Chemical structure of rhodamine B

Dyes get into the environment through the disposal of wastewater from textile, food, cosmetics, plastic, carpet, paint, pharmaceutical, and rubber, among other industries [1, 2, 4, 5, 8, 12, 13]. Consumptions of foods contaminated with dyes trigger diseases such as asthma, skin rashes, irregular heartbeat, muscle pain, and cancer [1, 6, 7]. Research associates the emergence and increase in cholera and cancer cases in Kenya with the consumption of untreated water from dams, lakes, and rivers [3].

Research has shown that adsorption is superior to other dye removal techniques [1, 18]. It is simple to design, affordable, readily available, easy to operate, universal, has high efficiency, and effectively removes dyes even in concentrated medium [1, 2, 4, 5, 8, 11, 12]. Therefore, adsorption is extensively applied to eliminate various contaminants from different matrixes by biochar, agricultural, and industrial materials as adsorbents [4, 5, 8, 12]. Some of the waste materials used include orange peels [2, 19]: rice husk [13, 18]; sawdust [20-22]; coconut shell [23, 24]; coir pith [24, 25]; fly ash [26, 27];, and corncob and barley husk [28].

This study investigated the adsorption efficiency for RhB on water hyacinth (leaves + stem)–MWCTS composite. Carbon nanotubes (CNTs) are effective adsorbents as a result of higher specific surface area and chemical reactivity than bulk materials of the same type [1, 8, 11]. Biochar is also a desired adsorbent for its properties, such as high specific surface area and porosity, and high cation exchange capacity [29]. It is hypothesized that combining the two materials (biochar–CNTs) will make a superior adsorbent for problematic organic contaminants [1, 8]. Besides, the utilization of water hyacinths will ultimately reduce the harmful effects of the plant, including reducing oxygen levels, blocking the penetration of light, and allowing the accumulation of poisonous gases such as hydrogen sulfide and ammonia in water bodies [30].

II. Experimental

Materials

Water hyacinths were collected from a swamp along Umoja Road, Ongata Rongai, Kajiado County in Kenya. MWCNTs, glutaraldehyde solution, and RhB were purchased from Hongwu Enterprise Group.

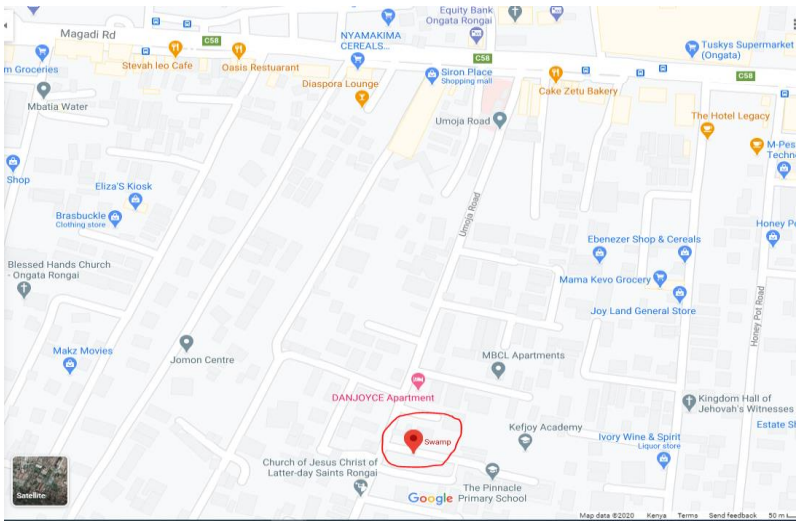

Figure 2: Map of the sampling site in Ongata Rongai, Kajiado County (1°24'00.5"S 36°45'05.3"E; -1.400146, 36.751483)

Hyacinths Biochar Preparation

The stem and leaves were separated from the roots, washed with tap water to remove soil, and rinsed with deionized water. The samples (stems and leaves) were dried at room temperature.

The fibres were then carbonized by slow pyrolysis (350 ºC) at Industrial Research and Development Institute (KIRDI), South C, Nairobi, Kenya. The biomass was sieved using a 72 μm pore-sized sieve at the State department of mining, Kenya.

Biochar–MWCNTs Composite Preparation

Two nanocomposites were prepared in the ratio; biochar–CNT (97.5:2.5) and biochar–CNT (95:5). The low percentage of CNT was selected to reduce the design cost yet tap the desired nanomaterial's adsorptive properties. Biochar, commercial MWCNTs, and the composites are shown in Figures 3 and 4. Biochar and CNT were mixed in a 75 ml beaker and ground to uniformity. 0.5 ml of the cross-linker (glutaraldehyde) was added, and the black product was ground to a soft homogenous paste. The paste was oven-dried at 80ºC for about 24 hours. The product was again ground into a fine powder and stored for utilization.

Adsorbate Preparation

One gram of RhB was dissolved in a litre of deionized water to make 1000 ppm of the dye (stock solution). The solution was mixed using a magnetic stirrer until all the RhB powder was dissolved. The working standards were prepared from this solution by serial dilution.

Dilutions were done using Equation 1.

Equation 1: $C_0V_0 = C_1V_1$

Where: C_0 is the stock solution concentration, ppm

C_1 is the working standard concentration, ppm

V_0 is the volume of the stock solution, ml

V_1 is the volume of the working solution, ml

Instrumentation

FTIR Analysis

FTIR spectra for the studied samples (Biochar and biochar–CNT composites) were collected using the spectrometer JASCO, FTIR-4700 from the pharmaceutical chemistry department, United States International University (USIU), Kenya, which scans the range from 400-4000 cm^{-1}. The adsorbent spectra were obtained by the KBr method pellet method before the adsorption of RhB. A soft, homogenous mixture of the KBr and each adsorbent in the ratio 5:1 was used.

XRD Analysis

The structural properties of the samples were characterized using X-ray Diffractometer (XRD) Bruker AXS model D2 phaser SSD16 at the State Department of Mining, Kenya. The sample was scanned between 2θ =10-52º, at a scan rate of 2º per minute.

Transmission Electron Microscope

The morphological characterizations were determined using a JEOL transmission electron microscope (JEOL, TEM 1010) at accelerating voltages of 100 kV. Samples were dispersed in ethanol, sonicated, and drop-dried on carbon-coated copper grids before the TEM analysis. Consequently, TEM images were captured using a Mega view 3 camera and then analyzed using iTEM software.

Sorption Method

Effects of Contact Time

The effects of contact time were conducted at room temperature and natural pH. 50 ml of 10ppm RhB was prepared in six different propylene containers for different contact times (10, 30, 60, 120, 180, and 210 minutes) by serial dilution from 1000 ppm. The containers were placed on a magnetic stirrer hot plate, and 50 mg of the biochar was simultaneously added to each container. The magnetic stirrer was added to each container, and the solutions were stirred at a minimum speed. The containers' content was removed from the magnetic stirrer hot plate after a predetermined time interval and centrifuged at 3500 RPM. The supernatant liquid was scanned from 200-900 nm, the wavelength selected, and concentrations of RhB were determined by UV/VIS. All the other readings were at this wavelength.

Effect of Adsorbent Dosage

Varying weights of the biochar (0.03, 0.1, 0.4, 0.7, 1.0, 1.3, 1.6, 1.9, and 2.2 grams) were measured into polypropylene containers at room temperature and natural pH. 50 ml of 10ppm RhB solutions were added to each

of the adsorbent doses simultaneously and stirred for 120 minutes. The contents were centrifuged at 3500 RPM, and UV/VIS determined the supernatant concentrations of RhB.

Effect of Dye Concentration

100 ml RhB solutions of different concentrations (100, 200, 300, 400, 500, and 600 ppm) were prepared in polypropylene containers from the stock solution at room temperature and natural pH. 1.0 gram of the biochar was added to each concentration simultaneously and stirred at minimum speed for 120 minutes. The contents were thereafter centrifuged at 3500 RPM, and the supernatant concentrations of RhB determined by UV/VIS.

Effect of Solution pH

The effect of pH on adsorption was tested by varying solution pH from 2 to 11 using 0.1M HCl and 0.1M NaOH. 100 ml of 50 ppm RhB solutions were prepared at room temperature and the pH regulated (pH 1, 2, 3, 4, 5, 6, 7, 8, 9, 10, 11). 1 gram of biochar was then added to each solution and stirred at minimum speed for 120 minutes. The contents were thereafter centrifuged at 3500 RPM and the supernatant concentrations of RhB determined by UV/VIS

Adsorption of RhB by CNT–Biochar Composites at Optimum conditions

The adsorption process was repeated using each of the proposed adsorbents; 100% biochar, 95:5% biochar–CNT, and 97.5:2.5% biochar–CNT at the obtained optimum conditions (contact time, 120 minutes, adsorbent dose, 1.6 grams, RhB concentration, 400ppm, and pH 3). Furthermore, the adsorption was done at varying temperatures (25, 30, 35, 40, and 45^{o}C) to identify the optimum temperature. The temperature of 100 ml of the RhB solutions was regulated using a hot plate and thermometer before adding the adsorbents. Similarly, the pH was adjusted before the introduction of the adsorbents.

III. Results And Discussions

Extraction of Biochar

Previous studies reported higher adsorption efficiencies for various contaminants, including RhB and heavy metals, by water hyacinth's aerial parts, compared to the roots [31, 32]. As a result, the plant's stem and leaves were used in this study.

About a kilogram of dry hyacinths (stem and leaves) were carbonized at 350 ^{o}C, yielding approximately 300g (30%) of the biochar. The biochar was sieved through a 72 µm pore size. This resonated with the findings that biochar sieved through 63.5 µm mesh had enhanced water retention capacity compared to ground biochar with similar particle size [33]. Furthermore, biochar sieved with a larger particle pore size mesh (2000-4000 µm) retains less water [33]. Sieved particles are more elongated compared to ground particles and thus have higher adsorption rates. The composition of the biochar and the biochar–MWCNT composites were obtained using FTIR spectroscopy, XRD diffraction, and TEM.

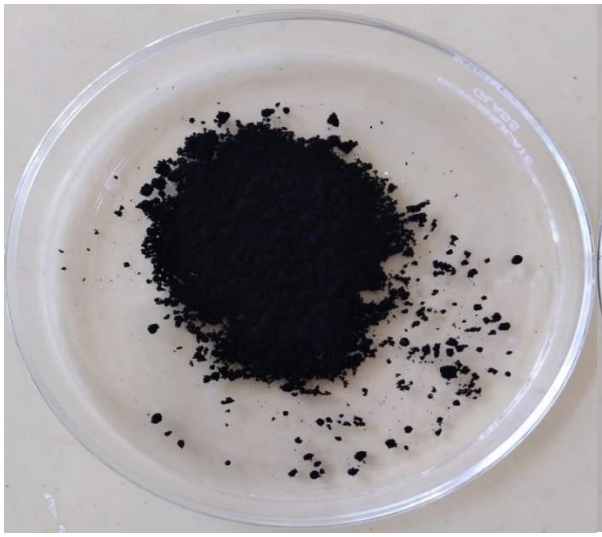

Figure 3: Commercial MWCNT

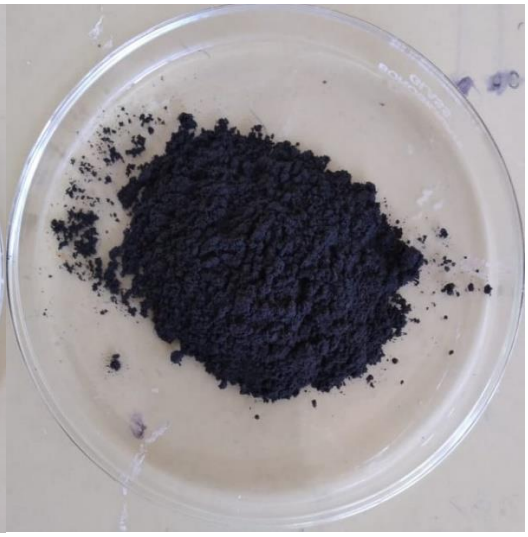

Figure 4: Biochar

Characterization of Adsorbents

FTIR Spectroscopy

Figures 5 presents the FTIR spectra of commercial MWCNT. Figures 6-8 present FTIR spectra of 2.5% CNT: 97.5% hyacinth's biochar, 5% CNT: 95% hyacinth's biochar, and 100 % hyacinth's biochar before adsorption, respectively. The spectra for 2.5% CNT: 97.5% hyacinth's biochar, 5% CNT: 95% hyacinth's biochar, and 100 % hyacinth's biochar after adsorption of RhB are shown in Figures 9-11, respectively.

For the commercial MWCNTs, the peak at 1546 cm^{-1} is due to the characteristic backbone C=C skeletal stretching of CNTs and was not observed in the 100% biochar adsorbents. The absorption bands at 1706 cm^{-1} and 2914 cm^{-1} are attributed to C=O stretching, and C-H Sp^3 hybridized stretching bonds, respectively [34]. The O-H (stretch, H-bonded) is observed between 3200-3600 cm^{-1} and the O-H (stretch, free) above 3700 cm^{-1} [34, 35]. Notably, the peak at 3224 cm^{-1} is most likely due to the O-H vibrations attributed to amorphous carbon. The peaks between 995-700 cm^{-1} are ascribed to the C-H out-of-plane bending vibrations or alkenes. Biochar introduces major peaks at 1032 cm^{-1} and 1400 cm^{-1}, which studies ascribe to C-O stretch and C-Hx (CH_2 or CH_3). Peaks at about 1450 cm^{-1} are attributed to CH_2 and those at around 1375 cm^{-1} to CH_3 [36, 37].

The major peaks in pure MWCNTs and 100% biochar are present in the composites, some with shifting wavelengths due to the weakening and strengthening of bonds. For example, all the O-H hydrogen bonding becomes weaker with oven heating and, as a result, shifts to higher wavelengths in the composites [38]. Similarly, the weak C=O at 1706 cm^{-1} representing the dipole-dipole interactions in the MWCNTs disappeared in the composites. This could be due to oven heating or the addition of carbon functional groups from the biochar and the dye.

In summary, comparative evaluation of the spectrum for MWCNTs, biochar, biochar–MWCNTs, before and after adsorption of RhB show that some peaks shifted, disappeared, and new ones were detected. This demonstrates the possible involvement of the adsorbent's surface functional groups in the sorption process.

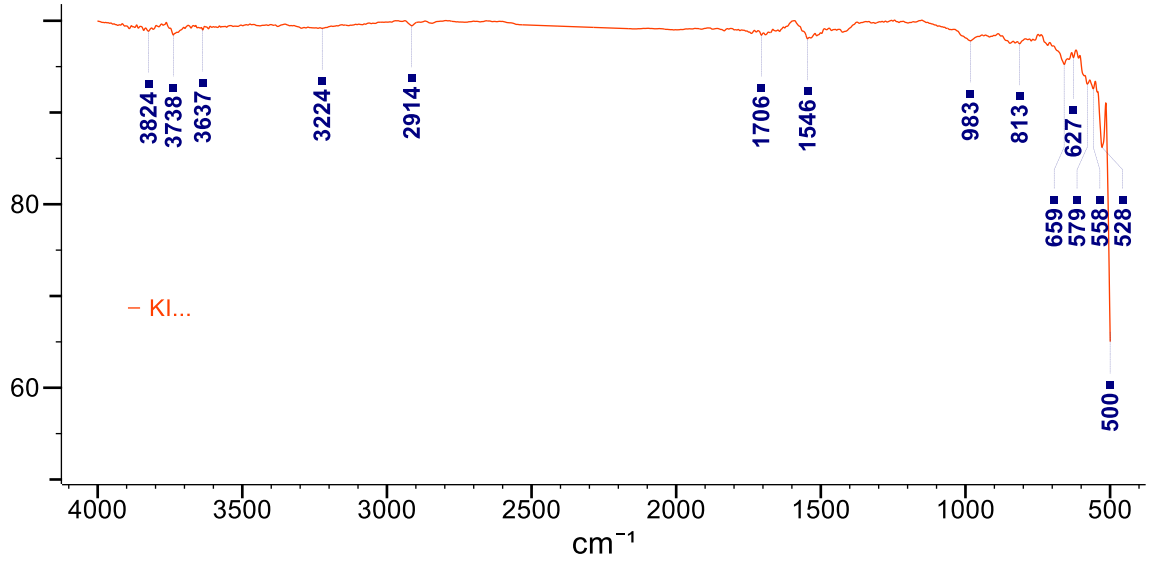

Figure 5: FTIR spectrum for Commercial MWCNT

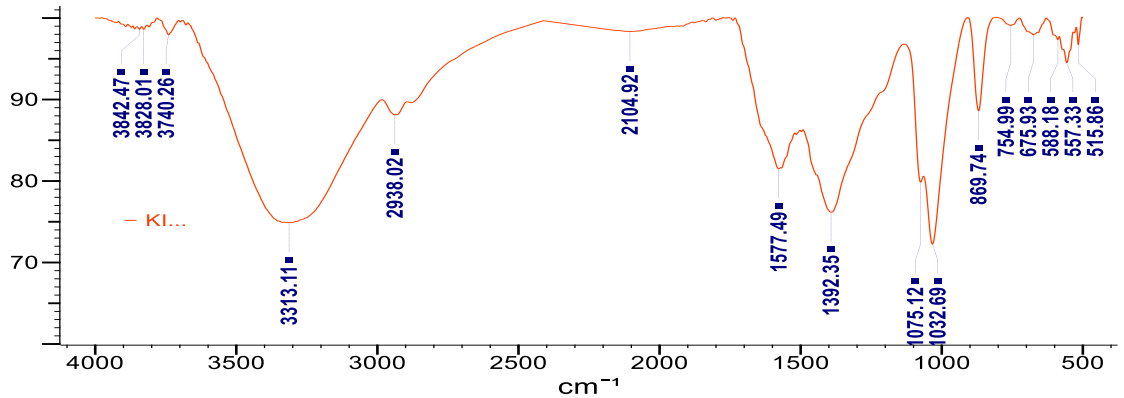

Figure 6: FTIR spectrum for 2.5% MWCNT–biochar composite before adsorption

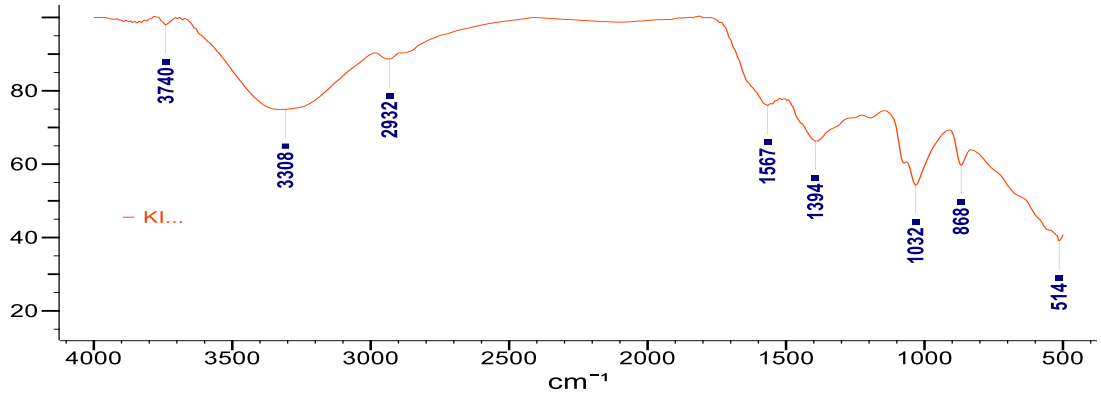

Figure 7: FTIR spectrum for 5% MWCNT–biochar composite before adsorption

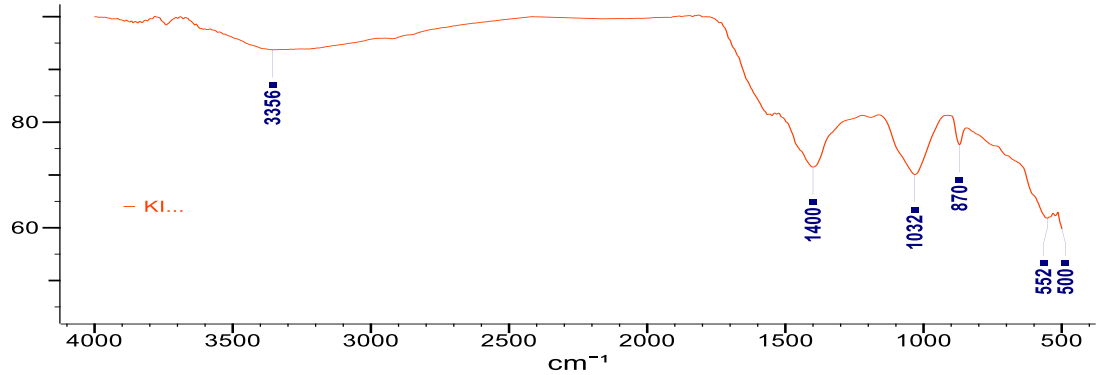

Figure 8: FTIR spectrum for biochar before adsorption

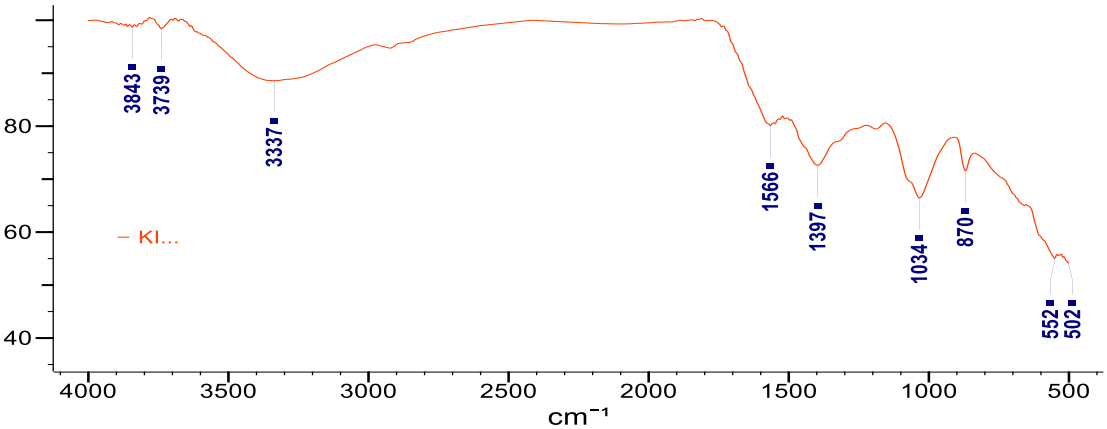

Figure 9: FTIR spectrum for 2.5% MWCNT–biochar composite after adsorption

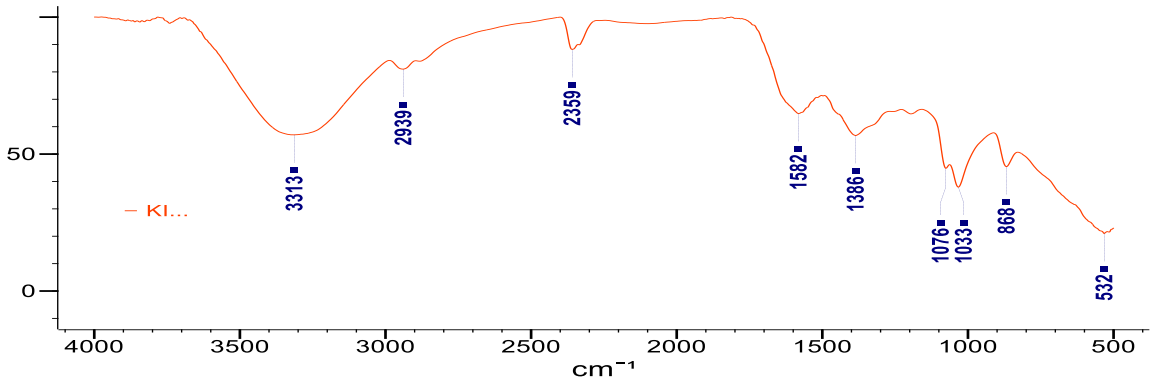

Figure 10: FTIR spectrum for 5% MWCNT–biochar composite after adsorption

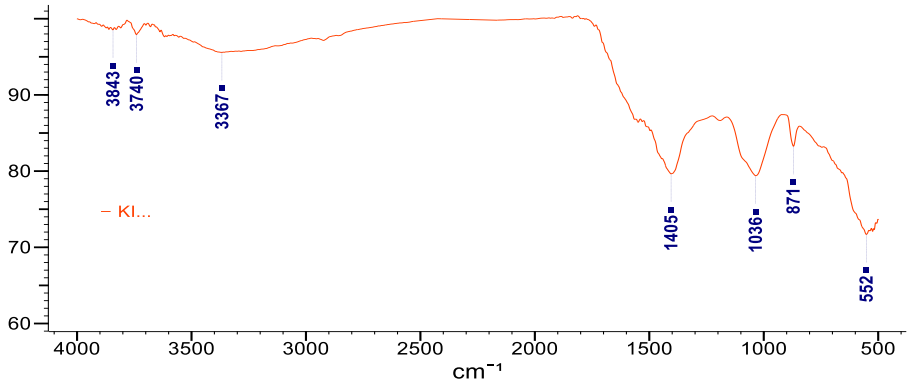

Figure 11: FTIR spectrum for biochar after adsorption

XRD Diffraction (XRD)

Figures 12-14 show the XRD pattern of 2.5% CNT, 5% CNT, and 100% biochar before adsorption. On the other hand, Figure 15-17 shows the XRD patterns after treatment with RhB dye. These materials (before and after adsorption) exhibit characteristic peaks at 28º and 40º, which previous studies related to (002) and (001) lattice planes of the hexagonal graphite phase [39, 40]. Normal graphite exhibits peaks at 2θ = 26.5º, and 40º. The slight shifts could result from the smaller interplanar spacing of the atoms in the lattice, the presence of different crystalline phases, and, impurities [40, 41]. There was no significant difference in positioning the peaks for 2.5% CNT, 5% CNT, and biochar. However, it is notable that the peaks after treatment have higher intensity due to the adsorption of RhD which contains carbon atoms.

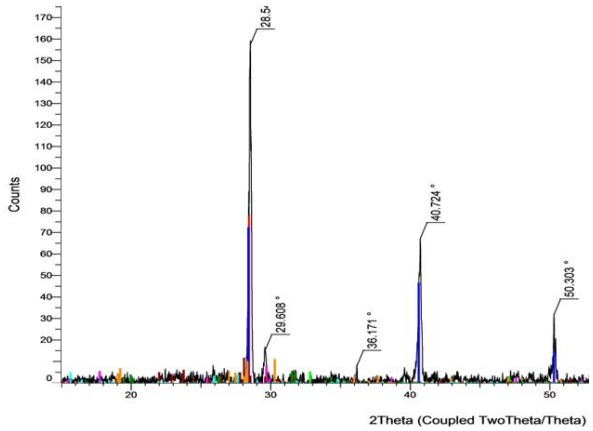

Figure 12: XRD spectrum for 2.5% MWCNT–biochar composite before treatment

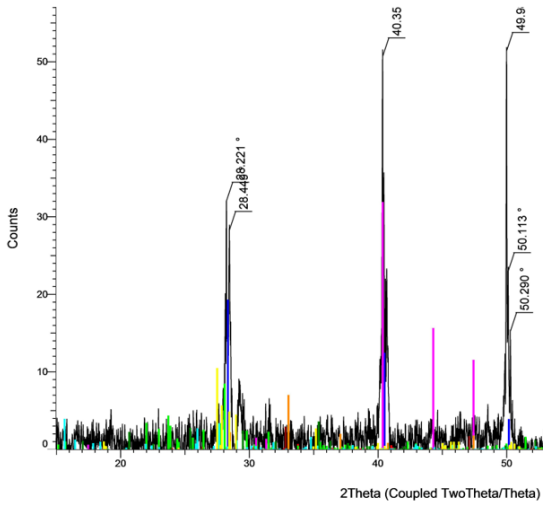

Figure 13: XRD spectrum for 5% MWCNT–biochar composite before treatment

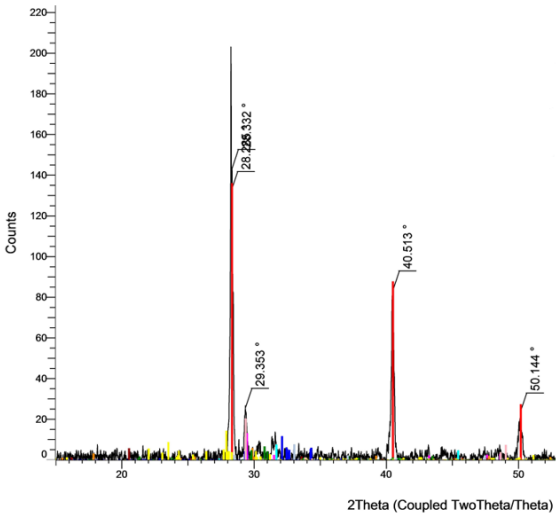

Figure 14: XRD spectrum for biochar before treatment

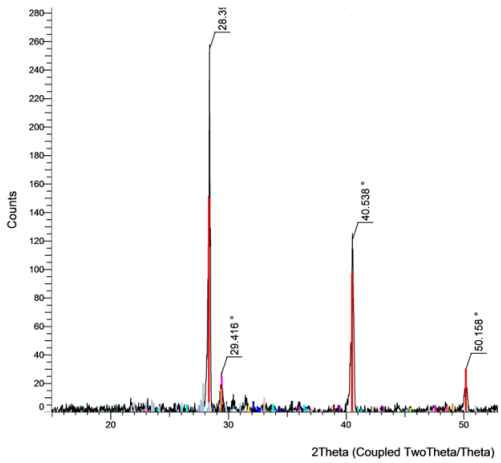

Figure 15: XRD spectrum for treated 2.5% MWCNT–biochar composite

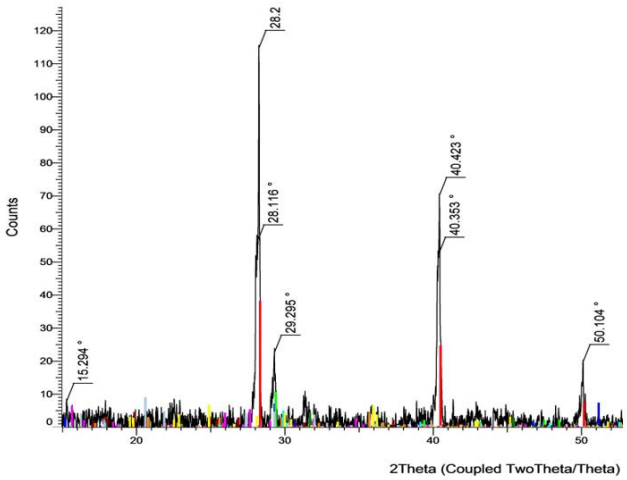

Figure 16: XRD spectrum for treated 5% MWCNT–biochar composite

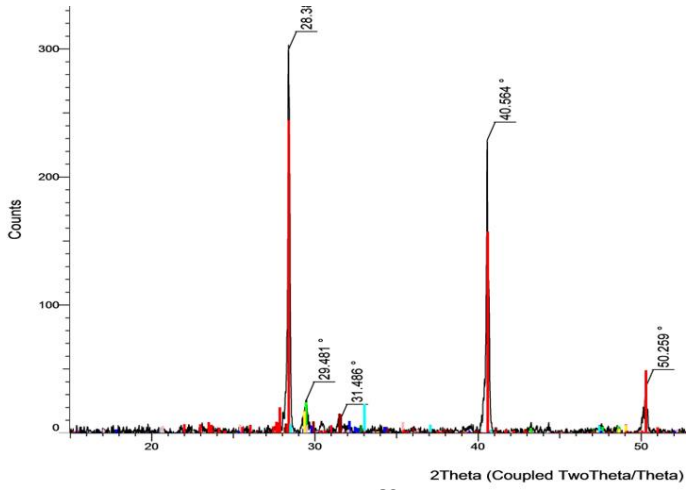

Figure 17: XRD spectrum for treated biochar

TEM Characterization

The morphological and structural characterization of the water hyacinth's biochar was obtained, as shown in Figure 18. The biochar was observed to show a large multiwall porous structure. Moreover, the carbon defects caused by heating during the pyrolysis process, and act as adsorption sites for RhD.

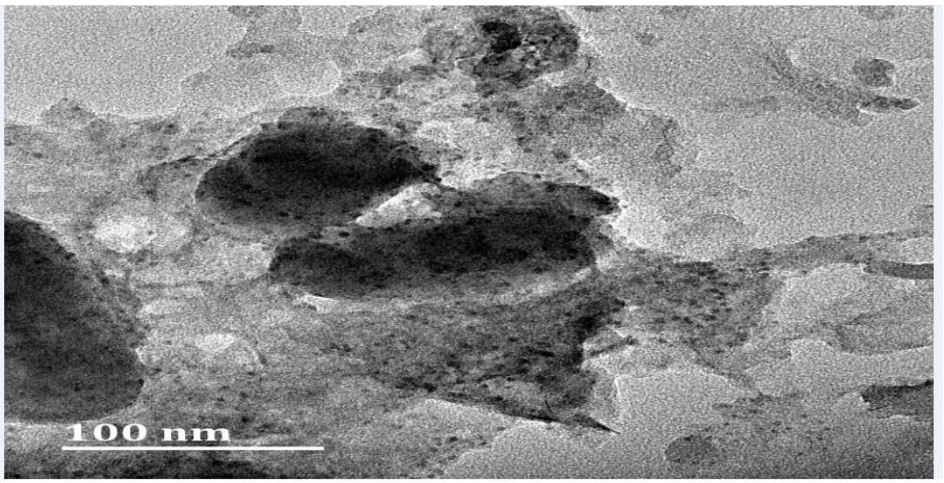

Figure 18: TEM image of the biochar

Adsorption Studies

Batch adsorption studies were carried out with respect to the contact time, adsorbent dose, and concentration of RhB dye. The quantity of RhB adsorbed (q_e) was calculated using Equation 2, and the percentage of adsorption from Equation 3 [43].

Equation 2: $$qe = \frac{(\mathrm{Ci}-Ce)}{m} \times v$$

Equation 3: $$ads.\% = \frac{Ci-Ce}{Ci} \times 100$$

Where *Ci* and *Ce* (mg/L) are the initial and equilibrium concentration of RhB,respectively, *m* (g) is the mass of the adsorbent, and *v* (l) the volume of RhB solution.
The RhB was absorbed at the wavelength of 254 nm.

Effect of Contact Time

Adsorption percentage was noted to increase with an increase in contact time until equilibrium was attained at 120 minutes, as demonstrated in Figure 19. This (120 minutes) was identified as the optimum contact time for RhB on hyacinths' biochar.

The fast adsorption rate at the initial minutes is because RhB was adsorbed by the adsorbent's exterior surface. When the adsorption on the exterior surface reached equilibrium, the dye was adsorbed through the internal surface, a phenomenon that takes a longer time to reach equilibrium.

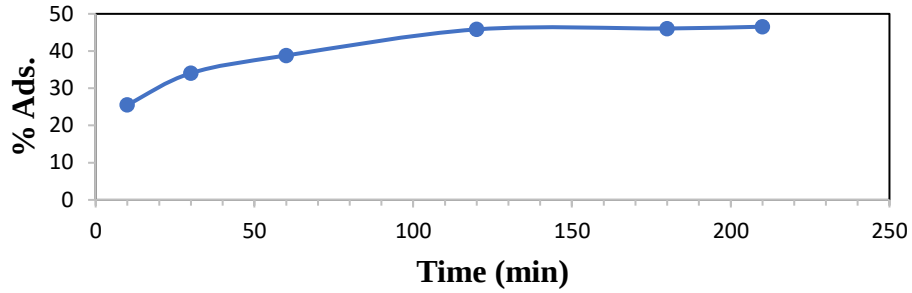

Figure 19: Effects of contact time on the adsorption percentage [conditions: RhB concentration (10ppm), adsorbent dose (50mg in 50ml), temperature (room temperature), pH (constant)]

Effect of Adsorbent Dosage

As indicated in Figure 20, the percentage removal of RhB increased with an increase in the adsorbent mass until equilibrium was attained at 1.6g. It increased from 34.7% at the initial dosage of 0.03 g to 94.34% at a dosage of 2.2 g. This is associated with the additional surface for interaction and adsorption sites. At equilibrium, all the available adsorption sites were filled up.

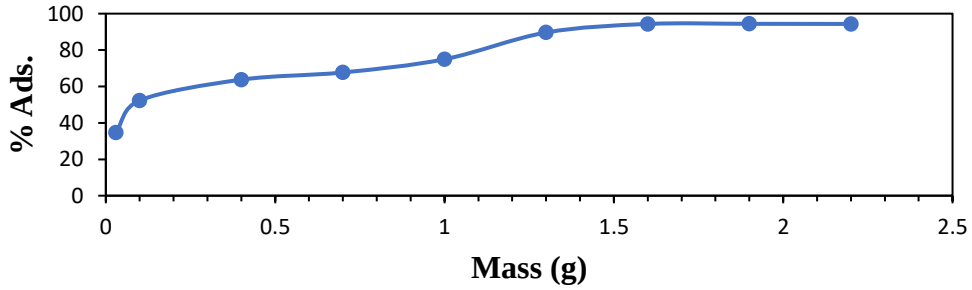

Figure 20: Effects of adsorbent dose on the adsorption percentage [conditions: RhB concentration (10 ppm), contact time (2 hours), Volume (50 ml), temperature (room temperature), pH (constant)]

Effect of Dye Concentration

The percentage adsorption increased with an increase in initial dye concentration up to 400 ppm, where equilibrium was attained. The adsorption capacity reached an equilibrium when all the available adsorption sites were filled. The highest percentage of adsorption was about 37% at 400 ppm, while the smallest was 12% at 100 ppm. This is demonstrated in Figure 21.

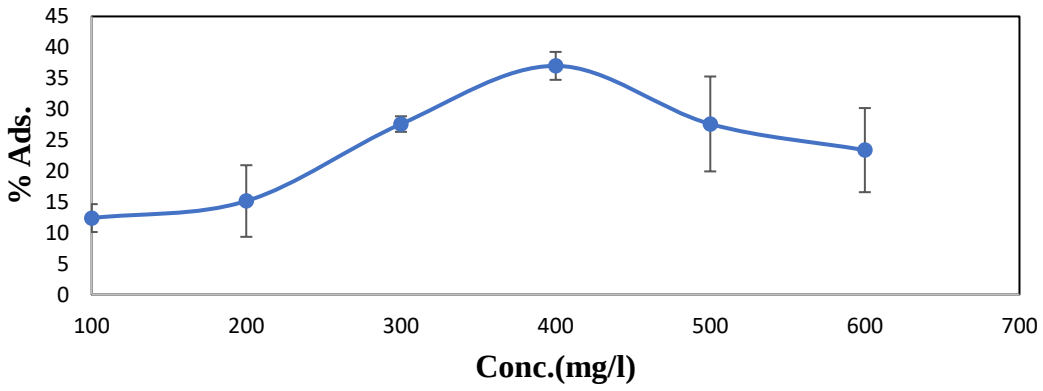

Figure 21: Effects of adsorbate concentration on the adsorption percentage [conditions: adsorbent dosage (10 g/l), contact time (2 hours), temperature (room temperature), pH (constant)]

Effect of Solution pH

The optimum percentage of adsorption was recorded at pH 3, as in Figure 22. This is contrary to the pH 6 obtained at the same conditions using acid-activated mango leaf as the adsorbent on RhB [44]. However, our results were close to another study where pH 4 was the optimum pH when dried water hyacinth leaves were used to remove RhB [31].

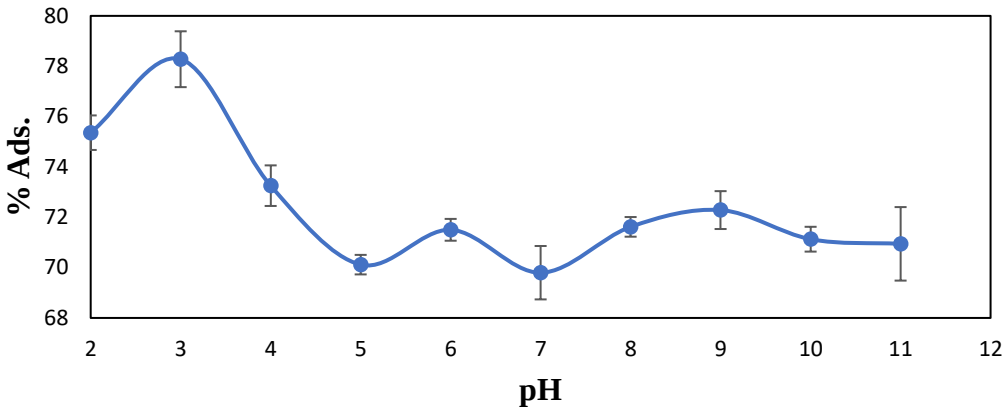

Figure 22: Effects of pH on the adsorption percentage
[conditions: contact time (2 hours) Adsorbent dose (10 g/L), the concentration of RhB (50 ppm), temperature (room temperature)

Adsorption by MWCNT–Biochar Composites at Different Temperatures

As in Figure 23, the adsorption percentage increased the amount of CNT in the composite. The adsorption rate was minimal for 100% biochar. The removal of more than 98% using ferrocene-functionalized MWCNT and 90% of RhB by acid-activated *Musa paradisiaca* biochar has been reported [45, 46].

The rate of adsorption decreased with an increase in temperature. Room temperature (~ 25^0C) was the optimum temperature within the range studied (room temperature, 303.15, 308.15, 313.15, and 318.15K). This agrees with other studies that achieved the maximum adsorption capacity of RhB on activated charcoal at 298.15K (210.2 mg/g) compared to 333.15K (196.4 mg/g) [47]. Moreover, an exothermic adsorption process for Basic Red 18 and Basic Blue 9 with an optimum temperature of 293.15K by activated sludge has been reported [48].

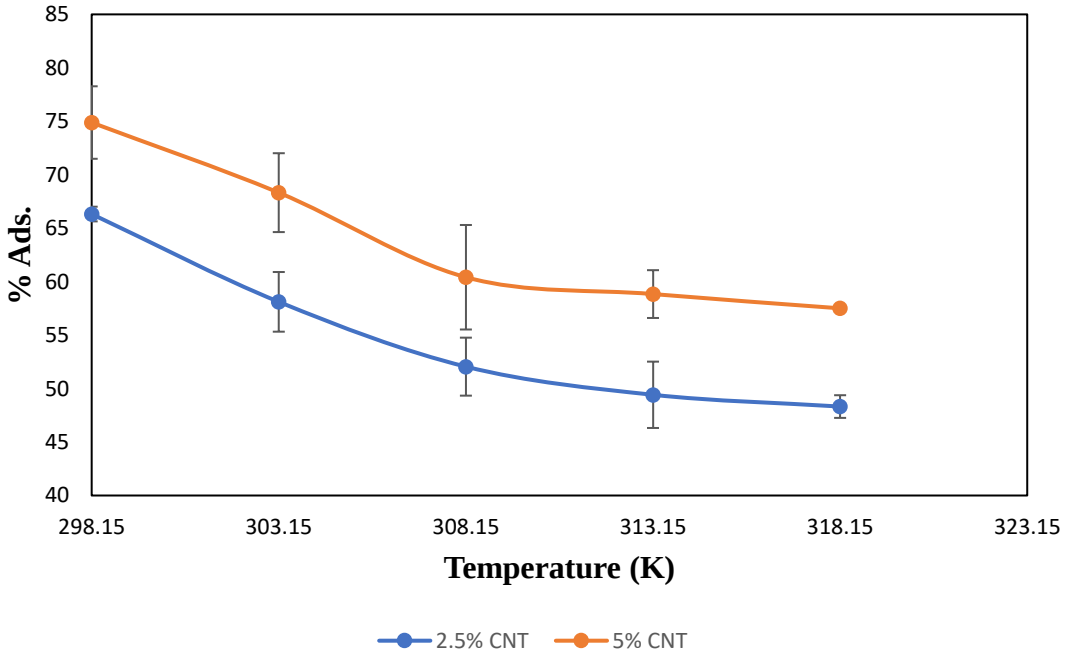

Figure 23: Effects of temperature on the adsorption percentage
[conditions: contact time (2 hours), Adsorbent dose (1.6g in 100ml), concentration of RhB (400 mg/l), pH 3]

The Van't Hoff thermodynamic plots for the adsorption of RhB on both nanocomposites were (Figures 24 and 25) plotted to determine whether the process was exothermic or endothermic. The Van't Hoff Equation measures the variation in the equilibrium constant with the temperature change and is driven from the Gibbs free energy as represented in Equations 4 and 5 [49].

Equation 4: $\Delta G^{O} = -RTIn(Kd)$

Equation 5: $\Delta G^{O} = \Delta H^{o} - T\Delta S^{o}$

Where: ΔG^{o} is the standard Gibbs free energy, ΔH^{o} is the standard enthalpy of the system, R is the universal gas constant (8.314 J K -1 mol^{-1}), T is the absolute temperature (K), and Kd is the thermodynamic equilibrium constant.

From Equations 4 and 5 [49].

Equation 6: $-RTIn(Kd) = \Delta H^{o} - T\Delta S^{o}$

Equation 7: $(In\ Kd) = \frac{\Delta H^{o} - T\Delta S^{o}}{-RT}$

Equation 8: $(In\ Kd) = \frac{-\Delta H^{O}}{RT} + \frac{\Delta S^{o}}{R}$… (Van't Hoff Equation)

Where: ΔS^{o} is the enthalpy change.

The Van't Hoff plot is made from In Kd versus 1/T, with $\Delta S^{o}/R$ and $-\Delta H^{o}/R$ as the y-intercept and the slope, respectively. The reaction is always exothermic when the plot is positive and negative for an endothermic reaction.

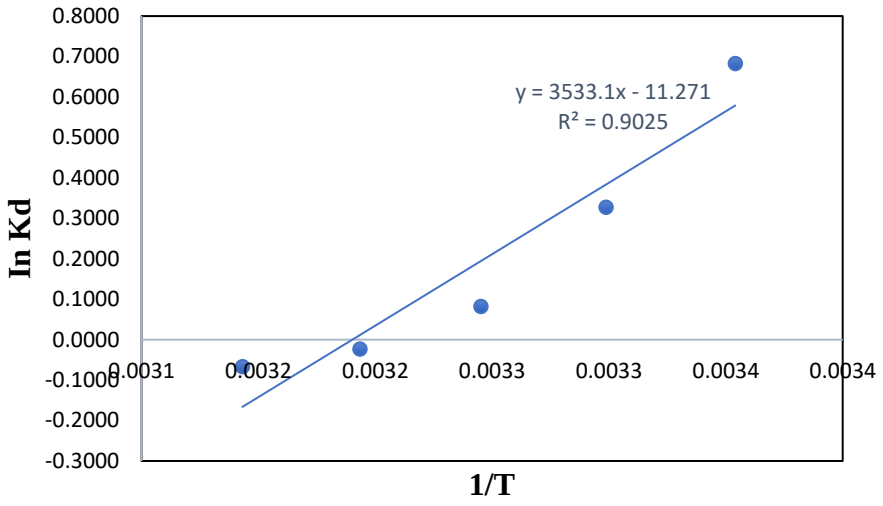

Figure 24: Van't Hoff thermodynamic plot for 2.5% MWCNT composite

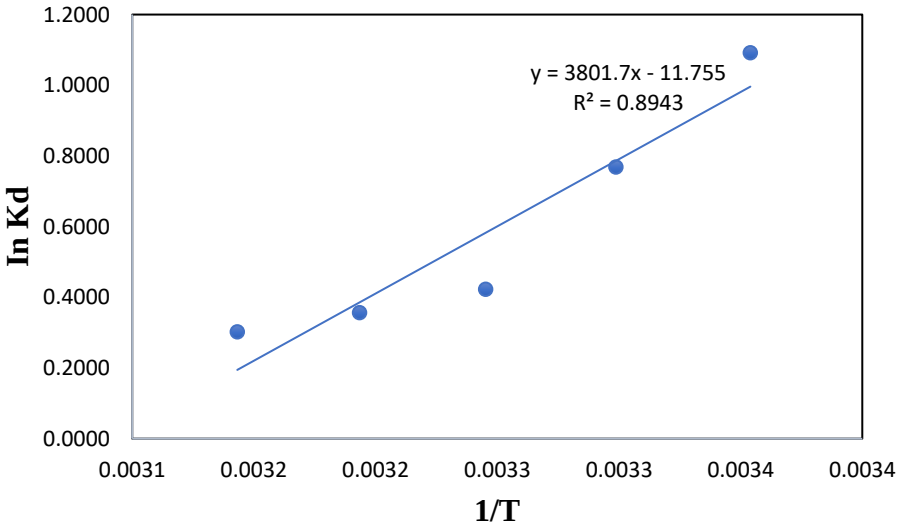

Figure 25: Van't Hoff thermodynamic plot for 5% MWCNT composite

Both the Van't Hoff plots for the adsorption of RhB onto 2.5% and 5% CNT were positive. Therefore, the adsorption reactions for this study were exothermic.

Adsorption Isotherms

In this study, RhB ions and the adsorbent interactions were described using Langmuir and Freundlich isotherms.

Langmuir Isotherm

The Langmuir isotherm model balances desorption and adsorption's relative rates and describes the surface coverage [50]. The adsorbent's open surface is proportional to adsorption, while the closed surface is proportional to desorption. Langmuir isotherm is expressed as in Equation 9 below:

Equation 9: $$\frac{Ce}{qe} = \frac{1}{qm.b} + \frac{1}{qm}Ce$$

Where: q_e is the quantity adsorbed at equilibrium (mg/g); C_e is the adsorbate concentration at equilibrium; q_m is the maximum amount of adsorbate for monolayer coverage (mg/g); b is the adsorption equilibrium constant (L/mg).

The Langmuir isotherm plot of $\frac{1}{qe} vs. \frac{1}{Ce}$, for the adsorption of RhB on hyacinth's biochar is shown in Figure 26.

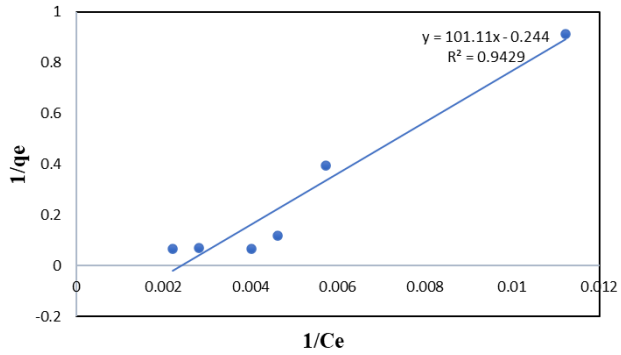

Figure 26: Linearized Langmuir plot for the adsorption of RhB

By comparing the Langmuir isotherm Equation to that in Figure 26 (our result);

Y = 101.11x-0.244

$1/q_m$ = -0.244

$1/q_m.b$ = 101.11

Therefore, b = -414.3552 (data does not fit the Langmuir since the value is negative).

Freundlich Isotherm

Freundlich isotherm explains adsorption on heterogonous surfaces and how the active sites and their energies are distributed [50]. Equation 10 shows the linear form of this isotherm [50].

Equation 10: $$\log qe = \log Kf + \frac{1}{n}\log Ce$$

Where: K_f and 1/n are the adsorption capacity (L/mg) and adsorption intensity, respectively.

The data obtained from the studies were used to fit the Freundlich isotherm, as in Figure 27.

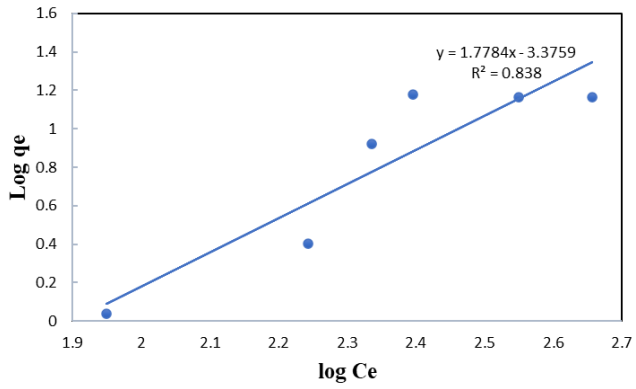

Figure 27: Linearized Freundlich plot for the adsorption of RhB

By comparing the Freundlich isotherm Equation to that in Figure 27 (our result);
Y = 1.7784x-3.3759
log K_f = -3.3759
1/n = 1.7784
Therefore, n = 0.5623 (The adsorption of RhB ions was described better by Freundlich isotherm)

Adsorption Kinetics

The data for the diffusion of RhB obtained were tested against the pseudo-first and pseudo-second-order kinetic models.

Pseudo-First Order

Also referred to as Lagergren, pseudo-first-order measures the adsorption of adsorbate onto the adsorbent regarding the first-order mechanism [51]. It is expressed in Equation 11.

Equation 11: $$\log(qe - qt) = \log Ce - \frac{K1}{2.303}t$$

where: q_e and q_t are the amounts of adsorbate adsorbed (mg/g) at equilibrium and at a specific time (time t): K_1 is the rate constant per minute (min^{-1}). The Pseudo-first-order model is described by a linear plot of log (q_e-q_t) versus t (Figure 28), where K_1 is obtained from the slope.
$K_1/2.303 = 0.6725$
$K_1 = 1.5488$

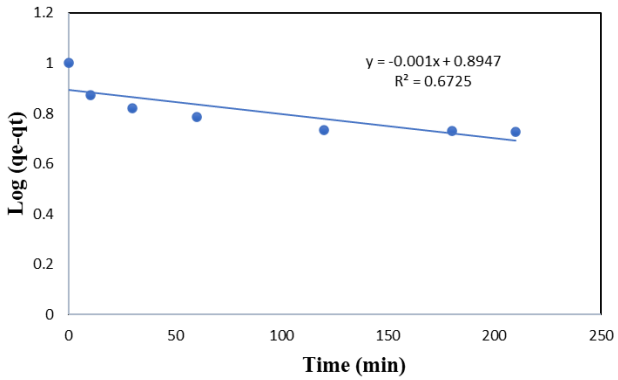

Figure 28: Linearized pseudo-first-order plot for the adsorption of RhB

Pseudo-Second Order

This model is based on the assumption that the adsorbate's rate of adsorption is proportional to the adsorbent's available sites [51]. It is expressed in Equation 12.

Equation 12: $$\frac{t}{qt} = \frac{1}{K2q_e^2} + \frac{1}{q_e}$$

Where: K_2 is the rate constant (gm/gmin). A linear plot of $\frac{t}{qt} vs\ t$ shows whether the adsorption kinetics obey the pseudo-second-order model (Figure 29), where K_2 is calculated from the intercept.
$K_2 = (0.2029)^2 * 2.4631$
$K_2 = 9.8618$

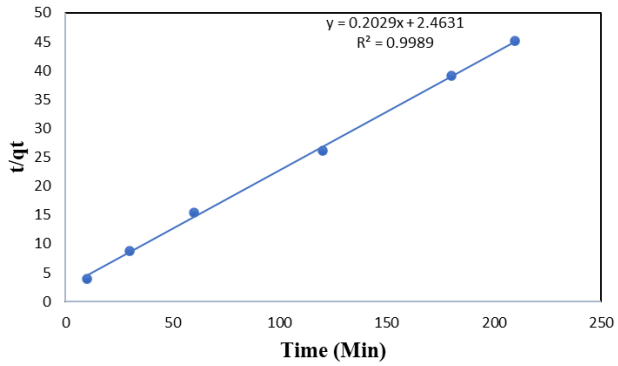

Figure 29: Linearized pseudo-second-order plot for the adsorption of RhB

The value of R^2 and adsorption constant for pseudo-second-order ($R^2 = 0.9989$; $K_2 = 9.8618$) were higher than that for pseudo-first-order ($R^2 = 0.6725$; $K_1 = 0.5488$). This suggested that the pseudo-second-order model better expresses the adsorption of RhB on water hyacinth's biochar.

IV. Conclusion

Biochar synthesized by slow pyrolysis and sieved to 72 µm was found effective for the adsorption of RhB. Furthermore, glutaraldehyde solution successfully cross-linked biochar and CNT to make composite. A much more efficient adsorbent for removing RhB was achieved by incorporating MWCNTs with hyacinth's biochar.

The findings reveal that the percentage adsorption of RhB increased with the amount of CNTs in the composite. For this reason, the adsorption percentage of 95:5% CNT–Biochar was higher than that of 2.5:97.5 CNT–biochar and 100% biochar, respectively.

The present study reports a maximum adsorption percentage of RhB on biochar, 2.5%, and 5% CNT to be 36%, 66%, and 75%, respectively. Adsorption was optimal at the following conditions: 2 hours contact time, 400 ppm of the adsorbate, 1.6g of the adsorbent, pH 3, and room temperature (~ 25^0C). The introduction of CNT enhanced the rate of adsorption

The batch adsorption studies provided essential information in terms of the contact time, adsorbent dose, solution pH, solution concentration, and temperature to remove RhB from the aqueous solution.

Characterization indicated possible involvement of the adsorbent's surface in the sorption process. Some FTIR peaks shifted while others were introduced or disappeared after treatment with RhB. On the other hand, the intensity of XRD peaks was enhanced after the sorption process due to the introduction of more carbon from the dye.

This study revealed that water hyacinths could be used to remove pollutants, such as dyes from aqueous solutions. These plants are abundantly available and problematic to the aquatic ecosystem. Moreover, they require minimal processing to be used as adsorbents of water pollutants.

Freundlich and the pseudo-second-order model better described the obtained data. This implies an empirical reaction involving the solute concentration on the adsorbent's surface and the solute's concentration in the aqueous solution.

References

[1] Ahmad, A., Et Al., Recent Advances In New Generation Dye Removal Technologies: Novel Search Of Approaches To Reprocess Waste Water. Rsc, 2015: P. 2-40.

[2] Arami, M., Et Al., Removal Of Dyes From Colored Textile Wastewater By Orange Peel Adsorbent: Equilibrium And Kinetic Studies. Elsevier, 2005: P. 371-375.

[3] Kithiia, S.M., Water Quality Degradation Trends In Kenya Over The Last Decade, Water Quality Monitoring And Assessment. Intech, 2012: P. 510-525.

[4] Singh, K. And S. Arora, Removal Of Synthetic Textile Dyes From Wastewaters: A Critical Review On Present Treatment Technologies. Critical Reviews In Environmental Science And Technology, 2011. 41(9): P. 807-859.

[5] Joshi, M., B. R, And R. Purwar, Colour Removal From Textile Effluents. Indian Journal Of Fibre & Textile Research, 2003: P. 239-255.

[6] Hassaan, M.A. And A.E. Nemr, Health And Environmental Impacts Of Dyes: Mini Review. American Journal Of Environmental Science And Engineering, 2017. 1(3): P. 64-65.

[7] Gürses, A., Et Al., Dyes And Pigments. 2016, Erzurum: Springer.

[8] Anastopoulos, I., Et Al., Use Of Nanoparticles For Dye Adsorption: Review. Journal Of Dispersion Science And Technology, 2017. 39(6): P. 836-844.

[9] Siringi, D.O., Et Al., Is Electrocougalation (Ec) A Solution To The Treatment Of Wastewater And Providing Clean Water For Daily Use. Arpn Journal Of Engineering And Applied Sciences, 2012. 7(1819-6608): P. 197-202.

[10] Kahenda, M., Wildlife At Risk As Sewage And Industrial Waste Choke Lake Nakuru. 2016, Standard Digital.

[11] Yonus, I.S., Et Al., Nanotechnologies In Water And Air Pollution Treatment. Environmental Technology Review, 2012. 1(1): P. 136-147.

[12] Go´Mez, V., M.S. Larrechi, And M.P. Callao, Kinetic And Adsorption Study Of Acid Dye Removal Using Activated Carbon. Elsevier, 2007: P. 1151-1156.

[13] Chuah, T.G., Et Al., Rice Husk As A Potentially Low-Cost Biosorbent For Heavy Metal And Dye Removal: An Overview. Elsevier, 2004. 175: P. 305-314.

[14] Saini, R.D., Textile Organic Dyes: Polluting Effects And Elimination Methods From Textile Waste Water International Journal Of Chemical Engineering Research, 2017. 9(1): P. 121-136.

[15] Jedynak, K., D. Widel, And N. Redzia, Removal Of Rhodamine B (A Basic Dye) And Acid Yellow 17 (An Acidic Dye) From Aqueous Solutions By Ordered Mesoporous Carbon And Commercial Activated Carbon. Colloids And Interfaces, 2019: P. 1-13.

[16] Garg, V.K., R. Gupta, And T. Juneja, Removal Of A Basic Dye (Rhodamine-B) From Aqueous Solutionby Adsorption Using Timber Industry Waste. Chemical And Biochemical Engineering Quarterly, 2005. 19(1): P. 75-80.

[17] El-Bindary, A.A., Et Al., Removal Of Reactive Blue 19 From Aqueous Solution Using Rice Straw Fly Ash J.Mater. Environ. Sci, 2016. 7(3): P. 1023-1036.

[18] Singh, D.K. And B. Srivastava, Basic Dyes Removal From Wastewater By Adsorption On Rice Husk Carbon. Indian Journal Of Chemical Technology, 2001. 8: P. 133-131.

[19] Sivaraj, R., C. Namasivayam, And K. Kadirvelu, Orange Peel As An Adsorbent In The Removal Of Acid Violet 17 (Acid Dye) From Aqueous Solutions. Elsevier, 2000. 21: P. 105-108.

[20] Garg, V.K., Et Al., Dye Removal From Aqueous Solution By Adsorption On Treated Sawdust. Elsevier, 2003. 89: P. 121-123.
[21] Garg, V.K., Et Al., Basic Dye (Methylene Blue) Removal From Simulated Wastewater By Adsorption Using Indian Rosewood Sawdust: A Timber Industry Waste. Elsevier, 2004. 63: P. 243-249.
[22] Khattri, S.D. And M.K. Singh, Removal Of Malachite Green From Dye Wastewater Using Neem Sawdust By Adsorption. Elsevier: Journal Of Hazadous Materials, 2009. 167: P. 1089-1093.
[23] Singh, K.P., Et Al., Color Removal From Wastewater Using Low-Cost Activated Carbon Derived From Agricultural Waste Material. American Chemical Society, 2003. 42(9): P. 1965-1975.
[24] Halim, H.N. And N.S. Yatim, Removal Of Acid Green 25 From Aqueous Solution Using Coconut Husk As Adsorbent. Iacsit Press, 2011. 12: P. 268-271.
[25] Namasivayam, C. And D. Kavitha, Removal Of Congo Red From Water By Adsorption Onto Activated Carbon Prepared From Coir Pith, An Agricultural Solid Waste. Elsevier: Dyes And Pigments, 2002. 54: P. 47-57.
[26] Wang, S., Y. Boyjoo, And A. Choueib, A Comparative Study Of Dye Removal Using Fly Ash Treated By Different Methods. Elsevier, 2005. 60: P. 1401-1407.
[27] Li, H., Et Al., Methylene Blue Adsorption Properties Of Mechanochemistry Modified Coal Fly Ash. Taylr & Francis Group, 2018: P. 1-7.
[28] Robinson, T., B. Chandran, And P. Nigam, Removal Of Dyes From An Artificial Textile Dye Effluent By Two Agricultural Waste Residues, Corncob And Barley Husk. Elsevier: Environmental International, 2002. 28: P. 29-32.
[29] Komkiene, J. And E. Baltrenaite, Biochar As Adsorbent For Removal Of Heavy Metal Ions [Cadmium(Ii), Copper(Ii), Lead(Ii), Zinc(Ii)] From Aqueous Phase. Int. J. Environ. Sci. Technol., 2016. 13: P. 472-480.
[30] Sterner, T., Lake Victoria Fish Stocks And The Effects Of Water Hyacinth. The Journal Of Environment & Development, 2009. 18(1): P. 62-77.
[31] El-Wakil, A.M., A. El-Maaty, And F. Awad, Adsorption Of Methylene Blue And Rhodamine B From Aqueous Solutions Using Dry Or Carbonized Water Hyacinth Plant. Journal Of Applied Sciences Research, 2013. 9(6): P. 3607-3617.
[32] Mishra, S. And A. Maiti, The Efficiency Of Eichhornia Crassipes In The Removal Of Organic And Inorganic Pollutants From Wastewater: A Review. Environmental Science And Pollution Research, 2017. 24(9): P. 7921-7937.
[33] Liao, W. And S.C. Thomas, Biochar Particle Size And Post-Pyrolysis Mechanical Processing Affect Soil Ph, Water Retention Capacity, And Plant Performance. Soil Systems, 2019. 3(14): P. 1-16.
[34] Nawaz, M.A.H., Et Al., One Step Assembly Of Thin Films Of Carbon Nanotubes On Screen Printed Interface For Electrochemical Aptasensing Of Breast Cancer Biomarker. Sensors, 2016. 16(10): P. 1-14.
[35] Lehman, J.H., Et Al., Evaluating The Characteristics Of Multiwall Carbon Nanotubes. Carbon, 2011. 49(2011): P. 2581-2602.
[36] Ibrahim, M., Molecular Spectroscopic Study Of Water Hyacinth Dry Matter. The Open Chemical Physics Journal, 2009. 2: P. 1-6.
[37] Osman, O., Et Al., Molecular Spectroscopic Study Of Water Hyacinth Collected From Different Media. Australian Journal Of Basic And Applied Sciences, 2010. 4(12): P. 6134-6139.
[38] Sharifpour, N., Et Al., Evaluation Of The Activated Carbon Coated With Multiwalled Carbon Nanotubes In Removal Of Ciprofoxacin From Aqueous Solutions. Applied Water Science, 2020. 10(140): P. 1-17.
[39] Banerjee, D., Et Al., Amorphous Carbon Nanotubes–Nickel Oxide Nanoflower Hybrids: A Low Cost Energy Storage Material. Acs Omega, 2018. 3: P. 6311-6320.
[40] Abdullah, M.P. And S.A. Zulkepli, The Functionalization And Characterization Of Multi-Walled Carbon Nanotubes (Mwcnts). Aip Conference Proceedings, 2015. 1678(050033): P. 1-5.
[41] Abdulrazzak, F.H. And A.F. Alkiam, Behavior Of X-Ray Analysis Of Carbon Nanotubes. Intechopen, 2019: P. 1-16.
[42] Ishimaru, K., Et Al., Characterization Of Sp2- And Sp3 -Bonded Carbon In Wood Charcoal. The Japan Wood Research Society, 2007. 53: P. 442-448.
[43] Oyetade, O.A., Et Al., Effectiveness Of Carbon Nanotube–Cobalt Ferrite Nanocomposites For The Adsorption Of Rhodamine B From Aqueous Solutions. Royal Chemical Society Of Chemistry, 2015. 5(29): P. 22724-227337.
[44] Khan, T.A., S. Sharma, And I. Ali, Adsorption Of Rhodamine B Dye From Aqueous Solution Onto Acid Activated Mango (Magnifera Indica) Leaf Powder: Equilibrium, Kinetic And Thermodynamic Studies. Journal Of Toxicology And Environmental Health Sciences, 2011. 3(10): P. 286-295.
[45] Adekola, F.A., S.B. Ayodele, And A.A. Inyinbor, Efficient Rhodamine B Removal Using Acidand Alkaline-Activated Musa Paradisiaca Biochar. Polish Journal Of Environmental Studies, 2019. 28(5): P. 3063-3070.
[46] Rabti, A., Et Al., Ferrocene–Functionalized Carbon Nanotubes: An Adsorbent For Rhodamine B. Chemistry Africa, 2019. 2: P. 113-122.
[47] Maneerung, T., Et Al., Activated Carbon Derived From Carbon Residue From Biomass Gasification And Its Application For Dye Adsorption: Kinetics, Isotherms And Thermodynamic Studies Bioresource Technology, 2015. 200: P. 350-359.
[48] Gulnaz, O., Et Al., Sorption Of Basic Dyes From Aqueous Solution By Activated Sludge. Journal Of Hazardous Materials, 2004. 108(3): P. 183-188.
[49] Inyinbor, A.A., F.A. Adekola, And G.A. Olatunji, Adsorption Of Rhodamine B Dye From Aqueous Solution On Irvingia Gabonensis Biomass: Kinetics And Thermodynamics Studie. South African Journal Of Chemistry, 2015. 68: P. 115-123.
[50] Ayawei, N., A.N. Ebelegi, And D. Wankasi, Modelling And Interpretation Of Adsorption Isotherms. Journal Of Chemistry, 2017. 2017(3039817): P. 1-11.
[51] Kajjumba, G.W., Et Al., Modelling Of Adsorption Kinetic Processes—Errors, Theory And Application. Advanced Sorption Proces Application, 2019: P. 1-19.